Full length article

Liquid-crystal active lens: application to image resolution enhancement

Vincent Laude [1], Carine Dirson

Thomson-CSF, Corporate Research Laboratory, Domaine de Corbeville, F-91404 Orsay cedex, France

Received 3 November 1998; received in revised form 3 February 1999; accepted 23 February 1999

Abstract

The liquid-crystal active lens combines a liquid-crystal spatial light modulator (LC-SLM) with an objective lens. The LC-SLM controls the phase in a pupil plane of the lens, and thus modifies arbitrarily, although within a limited dynamic range, the transfer function of the system. We demonstrate that a liquid-crystal active lens can improve the resolution of an imaging system that is not diffraction limited, i.e. if the detector pixel size is larger than the Airy pattern of the optics. This is achieved by micro-scanning the detector plane to $p \times p$ sub-pixel positions, combining the resulting sub-images in one larger image, and then deconvolving numerically the latter. Hence the number of pixels in the image is increased by a factor of $p \times p$. This principle is demonstrated experimentally, and the degradation of image quality as a function of the resolution enhancement factor p is discussed. © 1999 Elsevier Science B.V. All rights reserved.

Keywords: Liquid-crystal active lens; Spatial light modulators; Resolution enhancement

1. Introduction

It is well-known [1,2] that the resolution of an optical imaging system is ultimately limited by diffraction, and that the smallest observable feature is roughly the size of the Airy diffraction pattern. Super-resolution is usually understood as the possibility of accessing details of the observed object that lie beyond the diffraction limit. However, in practical imaging systems, and especially when using 2D sensors like CCD cameras, the pixel size sets another limit to the resolution that in many practical cases is more stringent than the diffraction limit.

In this paper, we restrict our attention to the case when the size of the diffraction pattern is much smaller than the size of the detection pixels, and we try and recover an image with a resolution higher than that of the 2D sensor, i.e. we want to see details that are smaller than the detection pixel pitch. Now the only information available is the sampled images or frames given by the detector itself. Then it is possible to obtain a higher resolution image from a sequence of frames from the same scene only if some different distortion of the scene occurs before detection and sampling of each frame. Such an operation can be achieved by micro-scanning the detector plane [3,4], i.e. a high resolution image is obtained from low resolution frames of the same scene where each frame is offset by a subpixel displacement. In other words, this is a deconvolution problem where the convolution kernel is synthesized by combining the same pixel shape at different locations. If the subpixel displacements are known exactly, then the convolution kernel can be computed without error, and a correct deconvolution obtained. The main limitations arise in practice from acquisition noise and the limited
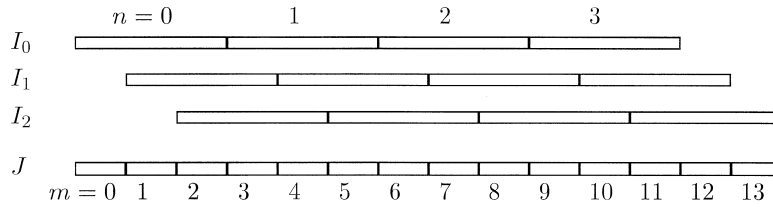
¹ Corresponding author. E-mail: laude@thomson-lcr.fr

Fig. 1. Schematic representation of the principle of resolution enhancement using micro-scanning. $p = 3$ in this example. Three images I_0, I_1 and I_2 of the same scene are acquired with respectively 0, 1/3 and 2/3 sub-pixel displacement. From these data, the high resolution image J must be reconstructed.

accuracy with which the subpixel displacements are known [5]. It is essential for the previously described method to be applicable that a precise and reliable micro-scanning device be used. Even though in theory either the detector or the projected image can be moved, it is generally faster to steer the projected image. Usual solutions involve steering mirrors or prisms. However, a programmable solution with no moving mechanical parts is certainly desirable, provided subpixel accuracy can be maintained. It is the purpose of this paper to introduce such a solution.

Takaki et al. [6] proposed to combine a liquid-crystal spatial light modulator (LC-SLM) with an objective lens, and named this arrangement a liquid-crystal active lens. The LC-SLM controls the phase in a pupil plane of the lens, and thus modifies arbitrarily, although within a limited dynamic range, the transfer function of the system. Using a parallel-aligned LC-SLM designed for phase-only modulation, Takaki et al. demonstrated several programmable functions, including image shifting. Image shifting is obtained by displaying a Fresnel prism on the LC-SLM. It was further proposed [7] to use an inexpensive twisted-nematic LC-SLM of the type used in small televisions. The LC-SLM used provided phase-mostly modulation and 640×480 resolution in the VGA standard. As shown in Ref. [7], the quality of the function achieved by the liquid-crystal active lens depends mainly on the spatial frequency content of the desired phase function. Interestingly, the micro-scanning function only requires a slight modification of the transfer function of the liquid-crystal active lens, and thus can be obtained with high quality.

We have used the twisted-nematic liquid-crystal active lens system described in Ref. [7] to implement a resolution enhancement algorithm. The main benefit of this approach is that the subpixel displacements can be controlled very accurately simply by specifying the target phase image to be displayed onto the LC-SLM. This control is achieved on a pixel-by-pixel basis and with 640×480 resolution. In Section 2, we present the simple convolution model that is used to describe the micro-scanning operation, and a linear deconvolution filter is introduced. In Section 3, we investigate by numerical simulation the robustness of the deconvolution method to input noise and the influence of the sought resolution enhancement degree. In Section 4, we

report and discuss experimental results obtained with our liquid-crystal active lens system.

2. Simple resolution enhancement model

For the sake of simplicity, one-dimensional notations are used (Fig. 1), but generalization to two dimensions is straightforward. If the sensor has N pixels, and a resolution enhancement factor of p is sought, this means that the high resolution image J will have $p \times N$ pixels. If the pixel dimension is a in the sensor, the pixel dimension of the high resolution image will be a/p. Let us denote I_q the low resolution image obtained after a subpixel displacement of qa/p; I_q contains N pixels. If it is assumed that there is no gap between the sensor pixels, then

$$I_q(n) = \sum_{i=0}^{p-1} J(np + q + i) + N_q(n), \tag{1}$$

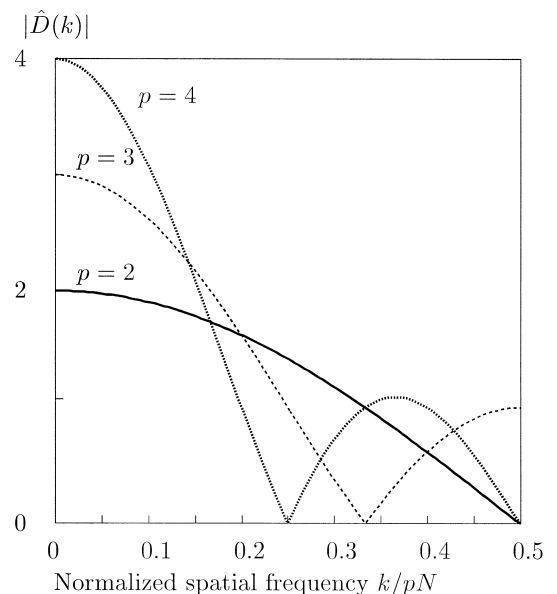where n varies between 0 and $N - 1$. Image N_q accounts

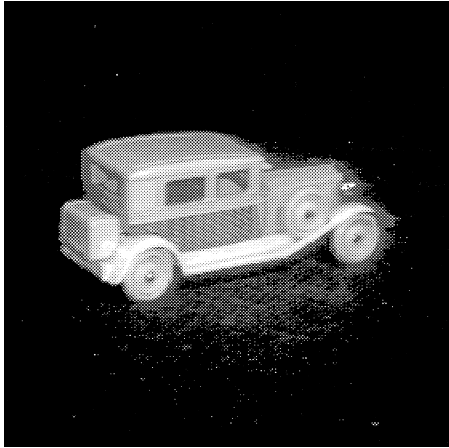Fig. 2. Plot of the modulus of the transfer function of micro-scanning given by Eq. (6).

Fig. 3. 256×256 image used in the numerical simulations.

for the acquisition noise, which is assumed to be uncorrelated. Next, the images I_q are mixed together to form image I defined by

$$I(m) = I_q(n) \quad \text{with } m = np + q. \tag{2}$$

In this equation, m varies between 0 and $pN - 1$, so that I has pN pixels like J. Eq. (1) can then be rewritten as

$$I(m) = \sum_{i=0}^{p-1} J(m + i) + N(m), \tag{3}$$

where the high resolution noise image N was formed from the low resolution noise images N_q using Eq. (2). Note that noise N is uncorrelated since the N_q are assumed uncorrelated. It is clear from Eq. (3) that the mixed image I is the result of the correlation of J with a kernel D such

that $D(m) = 1$ for $m = 0, \ldots, p - 1$ and $D(m) = 0$ elsewhere:

$$I(m) = [D \star J](m) + N(m). \tag{4}$$

Using the notation $\hat{(\ )}$ for Fourier transforms, Eq. (4) yields

$$\hat{I}(k) = \hat{D}^*(k)\hat{J}(k) + \hat{N}(k). \tag{5}$$

Written in this form, it is seen that the mixed image I has the same spectral content as the high resolution image J, but filtered by $\hat{D}(k)$ which is readily seen to be

$$\hat{D}(k) = \exp(-2i\pi(p-1)k/pN)\frac{\sin(\pi k/N)}{\sin(\pi k/pN)}. \tag{6}$$

The modulus of this function is plotted on Fig. 2. The action of D is clearly to enhance low frequencies and to lower high frequencies, but its most disturbing feature is the disappearance of all the spectral content of J near the zeros of $\hat{D}(k)$, in the vicinity of which only acquisition noise remain. As a consequence, the amount of information lost will depend on the strength of the acquisition noise.

The computation of an estimate J_e of the high resolution image J from the data I obtained via micro-scanning has been tackled from different points of view in the literature (see e.g. Refs. [5,8] and references therein). For the sake of simplicity, we will use a linear frequency domain approach, in which a deconvolution filter $\hat{H}$ is applied to $\hat{I}$ to yield the estimate:

$$J_{\hat{e}}(k) = \hat{H}(k)\hat{I}(k). \tag{7}$$

The Wiener filter is well-known to optimize the signal-to-noise ratio, but requires that the spectral density of J be known at least roughly. We use the following simple filter
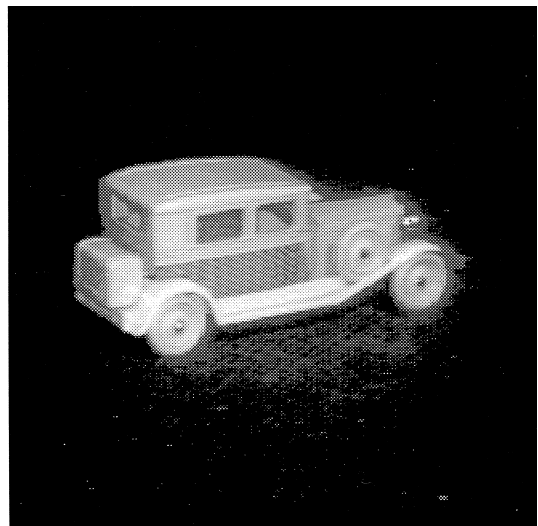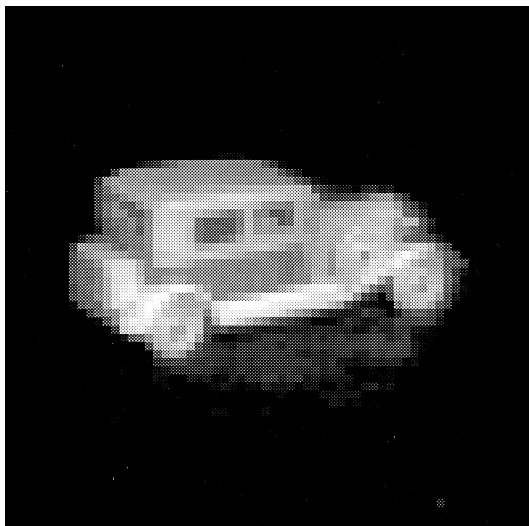

Fig. 4. Numerical simulation of resolution enhancement. (a) Example of a low resolution frame $I_q(p = 4)$ obtained from the image of Fig. 3 with no added input noise. (b) Reconstructed image J_e.

that depends on a single parameter s that is tuned depending on the strength of the noise:

$$\hat{H}(k) = \frac{\hat{D}(k)}{\max\left(|\hat{D}(k)|^2, s^2\right)}. \qquad (8)$$

The underlying idea is to discriminate between spatial frequencies for which useful information is expected, i.e. when the power spectral density $|\hat{D}(k)|^2$ exceeds a certain threshold s^2, and frequencies for which almost only noise is expected. The next section presents the robustness of this deconvolution filter to input noise and the resolution enhancement factor.
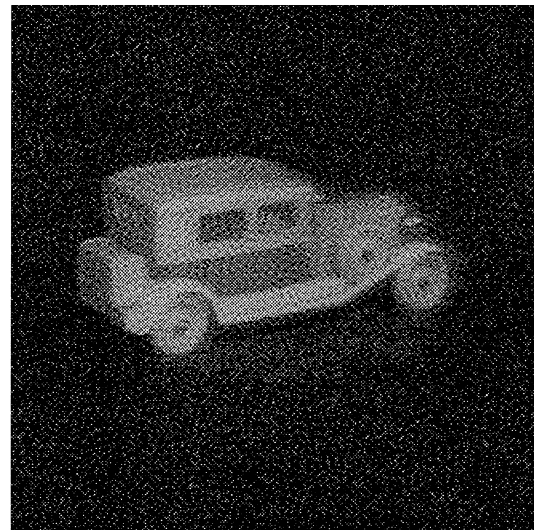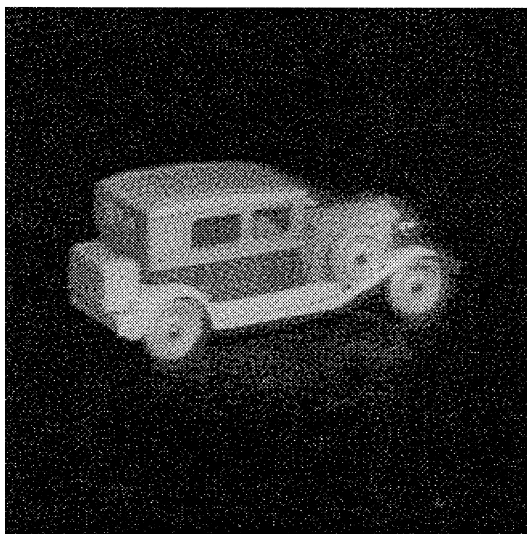
3. Numerical simulations

The image used for the numerical simulations is shown on Fig. 3. The $p \times p$ micro-scanned low resolution images are created from the image of Fig. 3 by averaging $p \times p$ pixels according to Eq. (1), and adding uncorrelated white
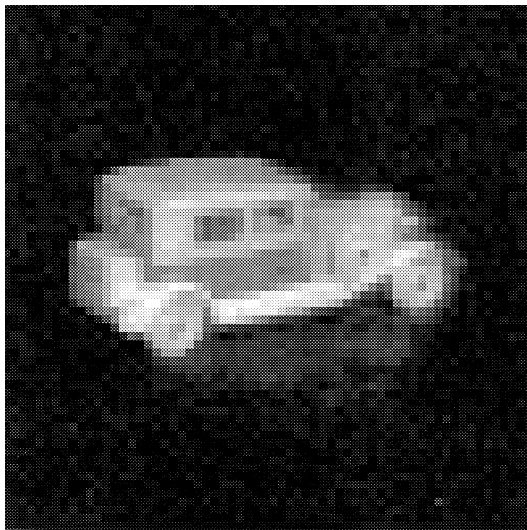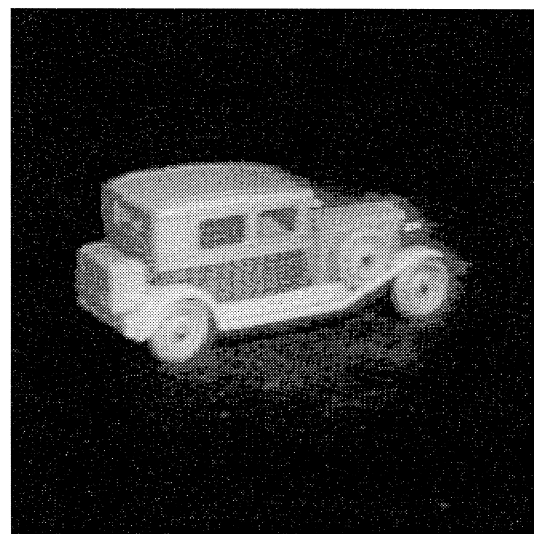

Fig. 5. Numerical simulation of resolution enhancement. (a) Example of a low resolution frame $I_q(p = 4)$ obtained from the image of Fig. 3 with added input noise with a variance $\sigma^2 = 4$. (b-d) Reconstructed image J_e with $s^2 = 0.2$, 1 and 6 respectively.

noise with zero-mean and variance σ^2 expressed in quantization units (256 quantization levels are used).

Fig. 4 illustrates that if no acquisition noise were present, then the reconstructed image would be identical to the ideal image but for numerical round-off errors ($p = 4$). This is expected since in this case the parameter s can be set very close to zero, so that almost no spatial frequencies are lost. In practical situations of course, noise is always present.

Fig. 5 illustrates the implications of the choice of the parameter s when noise is present. It can seen that with a resolution enhancement factor of 4, and with a noise with a variance of only $\sigma^2 = 4$, the reconstructed image can be strongly corrupted by noise if s is chosen too small. However, if it is chosen to large, the resolution enhancement will not be significant. s then appears as a trade-off parameter between resolution enhancement and reconstruction noise. Practically, its value has to be chosen by visual inspection of the reconstructed image.

The quality of the reconstruction is also very dependent on the resolution enhancement factor sought. This is illustrated on Fig. 6 where p is varied while the variance of the input noise is kept constant. In the left column are shown examples of low resolution frames for $p = 2$ and 8, while in the right column are shown the reconstructed images. Note that for $p = 8$, no less than 64 low resolution frames
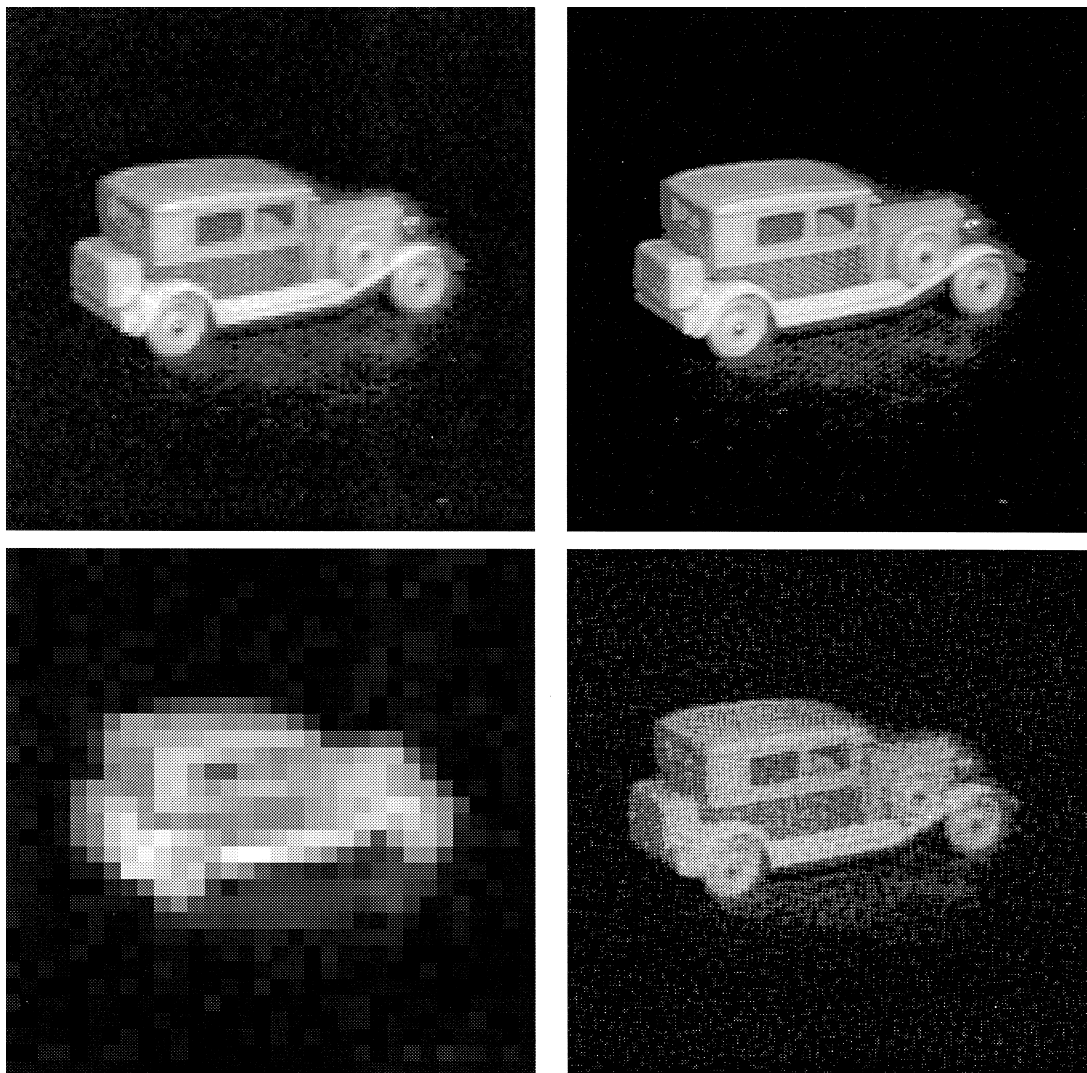

Fig. 6. Numerical simulation of resolution enhancement. Left column, from top to bottom: examples of low resolution frames I_q obtained from the image of Fig. 3 with added input noise with a variance $\sigma^2 = 4$, with $p = 2$ and 8 respectively. Right column, from top to bottom: reconstructed images J_e with $s^2 = 3$ and 20 respectively. Note that images (a) and (d) in Fig. 5 show comparable information for $p = 4$ and $s^2 = 6$.
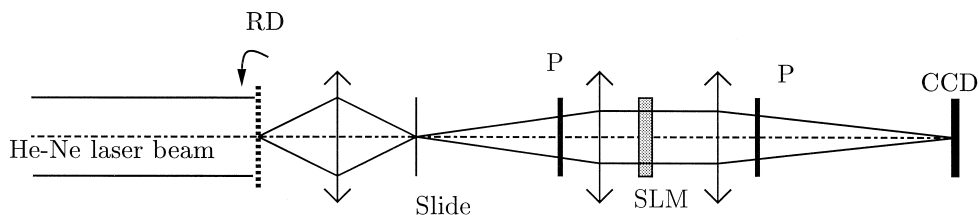
Fig. 7. Experimental set-up used to implement the resolution enhancement algorithm (see Ref. [7] for more details). RD: rotating diffuser; P: polarizer.

are required for the reconstruction. It is expected that since the number of low resolution frames increases quadratically with p, the noise robustness deteriorates rapidly.

4. Experiments

The experimental set-up used to implement the resolution enhancement algorithm was described in Ref. [7], and is schematized in Fig. 7. A collimated laser beam ($\lambda = 632.8$ nm) is incident upon a rotating diffuser that averages the speckle. The rotating diffuser in turn illuminates a transparent slide displaying a scene. The slide is imaged on a CCD camera via two doublets corrected from spherical aberration. In between the two doublets, a twisted-nematic liquid-crystal SLM controls the wavefront in a pupil plane, and provides the required sub-pixel displacements. The phase images sent to the SLM are Fresnel prisms which were described in Ref. [7]. They actually cause no loss in the spatial resolution of the imaging system provided the required displacements are small, which is always the case here. The spatial resolution is estimated to be of the order of 10 μm [7], which is just slightly less than the pixel pitch of the CCD camera.

The goal of the experiments was not actually to demonstrate an enhancement of the resolution of the CCD sensor, which was already almost at the diffraction limit, but to show that a sensor with less resolution could be enhanced
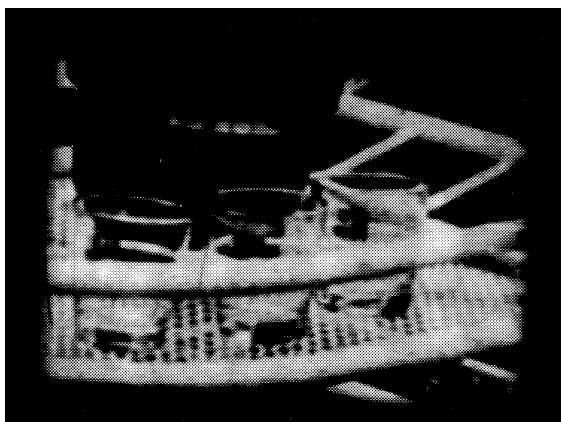
by a liquid-crystal active lens system. Fig. 8 shows the scene as seen by the CCD camera and acquired with a frame-grabber at a resolution of 320×240 pixels. This resolution is chosen so as to be twice above the diffraction limit. The scene represents glasses on a tray. As in the numerical simulations, low resolution images were generated by averaging $p \times p$ pixels for all required sub-pixel displacements. Fig. 9 displays some experimental results for $p = 2$, 4 and 8. All images are shown without any post-processing. It can be seen that a resolution enhancement is clearly obtained in all three cases, but that a spurious effect alters the quality of the image for $p = 8$. A mesh-looking structure appears after deconvolution that has exactly a period of p pixels. We attribute this effect to an error in the exact displacements achieved. Indeed, the convolution model of Eq. (1) clearly assumes that the pixel size is known exactly. Errors arise from an imprecise knowledge of the pixel pitches of the SLM and the CCD sensor, and probably more significantly of the focal length of the second lens in our experiment. Furthermore, additional errors are introduced by the frame grabber during resampling of the video signal sent by the CCD camera. The use of a numerical CCD camera would probably reduce notably this effect.

5. Conclusion

We have described a simple model of resolution enhancement and a deconvolution filter that can reconstruct a resolution-enhanced image from micro-scanned low resolution frames. The robustness of this deconvolution filter to input noise and to the resolution enhancement factor sought has been discussed. We have proposed to generate optically the required sub-pixel displacements without any moving mechanical parts using a liquid-crystal active lens. Our experiments demonstrate clearly an enhancement in the resolution, although a spurious effect appears with large resolution enhancement factors, that is probably connected to a systematic error in the displacements.

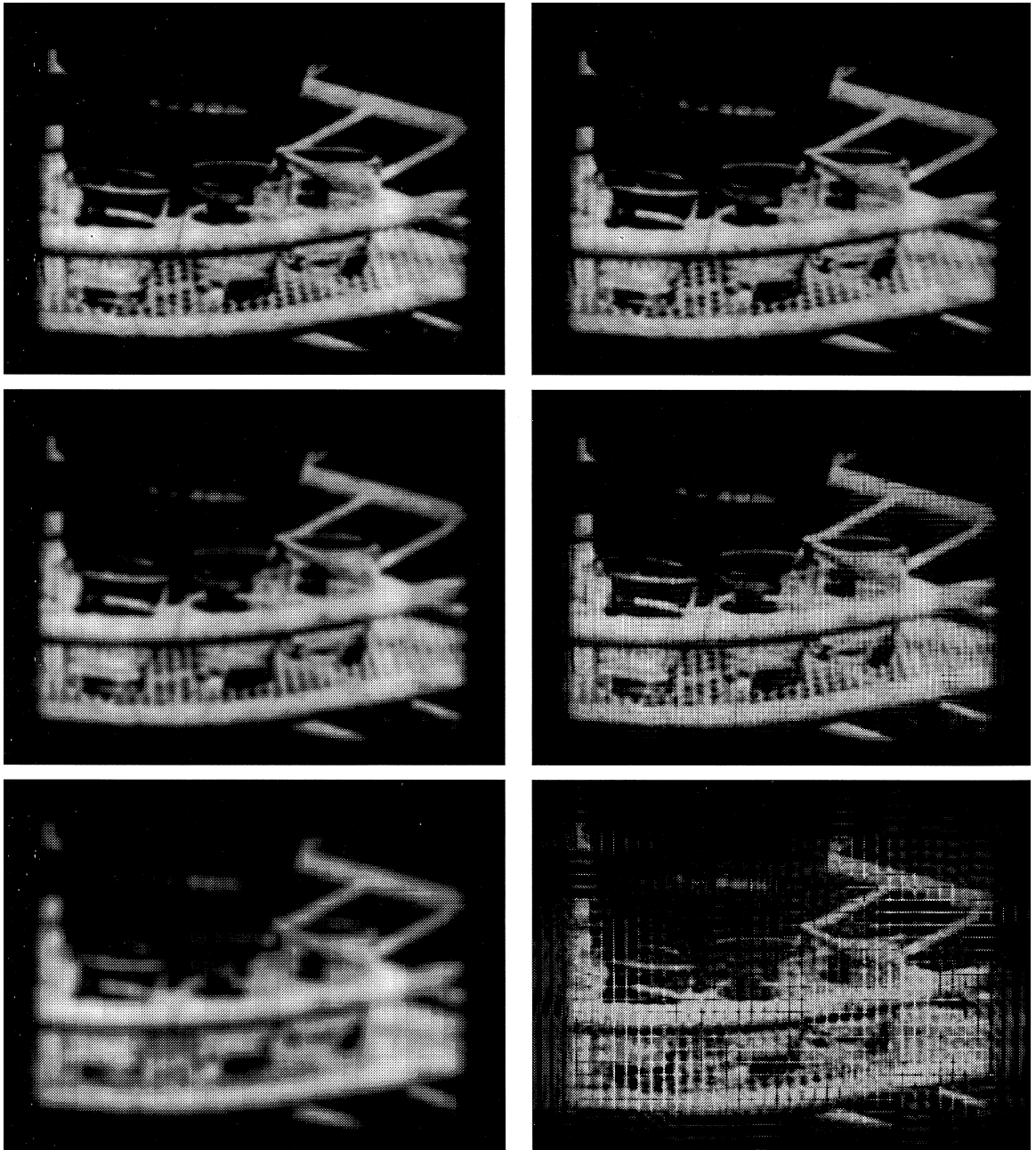Fig. 8. 320×240 image used in the experiments.

Fig. 9. Experimental implementation of resolution enhancement. Left column, from top to bottom: examples of low resolution frames I_q for $p = 2$, 4 and 8 respectively. Right column, from top to bottom: reconstructed images J_e with $s^2 = 15$, 15 and 20 respectively.

References

[1] J.W. Goodman, Introduction to Fourier Optics, McGraw-Hill, San Francisco, CA, 1968.

[2] M. Born, E. Wolf, Principles of Optics, Pergamon Press, New York, 1980.

[3] S. Pelleg, D. Keren, L. Schweitzer, Pattern Recognition Letters 5 (1987) 223.

[4] G. Jacquemod, C. Odet, R. Goutte, Signal Processing 26 (1992) 139.

[5] T. Nummonda, M. Andrews, R. Kakarala, Optics Comm. 108 (1994) 24.

[6] Y. Takaki, H. Ohzu, Optics Comm. 126 (1996) 123.

[7] V. Laude, Optics Comm. 153 (1998) 134.

[8] R.R. Schultz, R.L. Stevenson, IEEE Transactions on Image Processing 5 (1996) 996.